EVLA Memo 237

Validating VLA OTF Holography

Pedro P.B. Beaklini

December 5, 2024

Abstract

Radio astronomical holography is a technique of mapping the antenna surface to determine the accuracy of the reflector. It consists of using one antenna to map a point source while one or more additional antennas track that same point source to serve as reference measurements. At the VLA, the technique of point-and-shoot holography was developed over many decades of work by Rick Perley, Eric Greisen, et al., resulting in a total synergy between the method that gets the data and the software that analyzes it. In this memo, I will present the validation results of the on-the-fly holography technique, which was recently implemented at the VLA (motivated by the ngVLA prototype needs) and allows us to obtain antenna surface measurements in a much faster time scale.

1 Introduction

Holography has been done at VLA since the 90s (Kesteven 1994), and Rick's EVLA Memo 212 carefully describes the background, results, and math. It has been years of development and many iterations between Rick Perley and Eric Greisen to achieve the state of the art for the technique and develop a fast and reliable way to analyze the data in AIPS and to adjust the panels of each of the EVLA antennas, allowing high performance at high-frequency (K, Ka and Q bands).

Since I won't attempt to summarize or duplicate the analyses Rick has already detailed in his memo, I strongly encourage you to read Memo 212 (Perley 2021). It contains all the essential information, definitions, and data reduction steps for a comprehensive understanding. Here, I will briefly summarize holography in radio astronomy as the use of a reference antenna to obtain an illumination map and compute the surface deviations of a target antenna (Bennett et al. 1976). Although there are many approaches to getting holography maps – near-field (Mangum et al. 2006, Baars et al. 2007), far-field (Morris et al. 1988, Kestevan 1994) , satellites (Tarchi & Comoretto 1993, Serra et al. 2012) and even out-of-focus (Nikolic et al. 2007, Buffa et al. 2020, Cassanelli et al. 2024) – typically, the target antenna moves around a point astronomical source (a bright quasar) while the reference antenna keeps on the source. It is a powerful tool for describing the beam of the target antenna and checking its surface quality. Using the phase information to obtain the rms displacement of the surface, we can fit places with a high deviation and determine changes in the screw torque to improve the surface performance (Baars 2007). The term holography refers to a technique created by Dennis Gabor that uses laser diffraction and a reference beam to reconstruct the structure of a given material (a crystal) using amplitude and phase. This creative method earned Gabor the Nobel Prize in Physics in 1971.

Up to now, the only method used to perform holography measurements at the VLA is known as point-and-shoot holography (here also refereed as step holography). The moving antenna stops at each point of the point source map grid for 10 seconds, gathering information on amplitude and phase. Then, it moves to the following point. A significant amount of time is spent accelerating and decelerating the antenna. As an example, in a 43x43 grid, a total of 1809 points are observed, each one with 10 seconds, which takes a total of 5.1 hours. And there is still the calibration and pointing overhead. To obtain a holographic map with enough resolution to make a panel adjustment, we need at least 6 hours of VLA time.

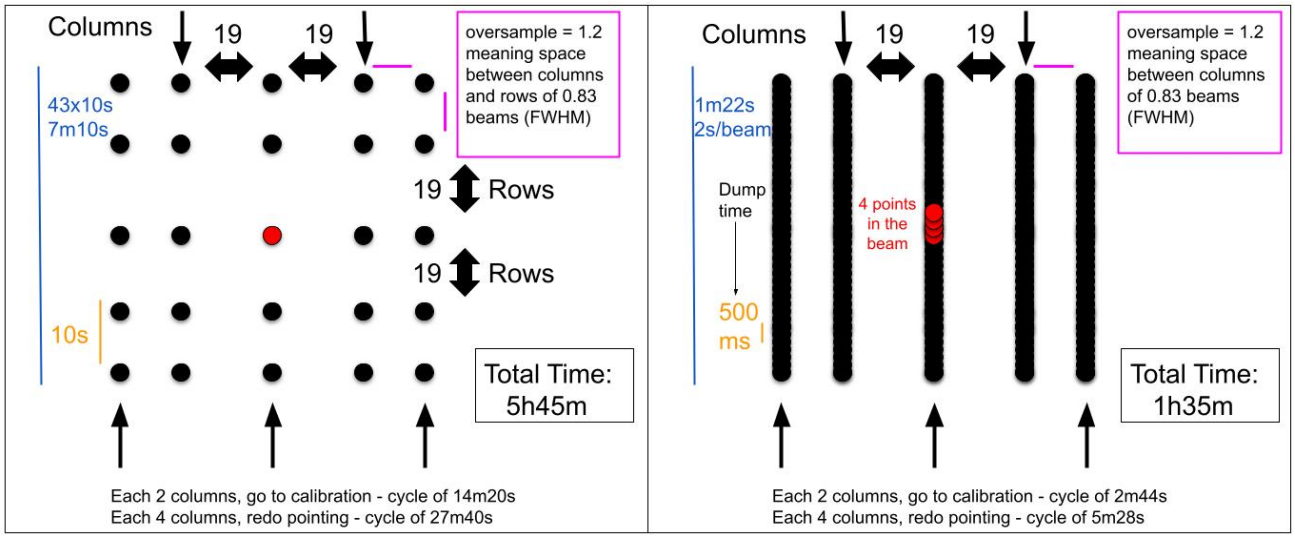

Figure 1: Schematic view of the two methods to perform holography, where columns represent elevation direction and rows azimuth direction. On the left: point-and-shoot holography with 43x43 grid. The antenna under measurement stops at each point for 10 seconds (which includes the slew time). The red point indicates the on-source position in the center of the grid. After each column, the antenna returns to its initial position in elevation and starts the following row in the opposite direction (down to the top). On the right: OTF holography, where the antenna moves continuously, scanning the target source in a raster pattern while acquiring data at the dump time rate. We get 4 points in the beam, and there is a dummy time of 6 seconds after each column when the antenna goes in the opposite direction (up to bottom).

Motivated by the ngVLA's need for a fast holographic measurement procedure to test the prototype antenna (see ngVLA Antenna Memo 12, Mangum 2022), the EVLA operations team started implementing the on-the-fly holography method hereafter OTF. On the OTF, the antenna does not stop at particular points; it keeps moving, scanning the source while the data is being recorded. With no need for acceleration and deceleration, the procedure is much faster than the usual holography, and the speed limitation is given by the time-on-source needed to obtain a reasonable map.

The changes on the executor that allowed OTF holography were made possible by Ryan Berthold, with the help and support of Ken Sowinski's expertise. The present memo describes the process of validating those changes on the executor, checking if the OTF holography reproduces the same results we obtain with the point-and-shoot holography. With the advantage of being faster, those changes on the executor are important to the ngVLA prototype and future EVLA holography.

2 OTF Antenna movement

In this section, I will add more details about the differences in the antenna movement between OTF and step holography. Both scripts are flexible, allowing the user to choose between various parameters to observe, like the direction of the movement, calibration cycle, time at each point, oversampling, etc. For a fair comparison between both methods, let's consider a holography to get panel adjustments, typically done at VLA at Ka-band in 40-ish square gridding, 1.2 beam oversampling, and 10 seconds in each observation point encompassing the slew time. Normally, we prefer to move through the elevation direction because a VLA antenna moves faster in elevation than in azimuth.

Figure 1 shows a schema comparing the antenna movement between the methods. On the step holography, considering a 43x43 grid, each row takes 7m10s (43 X 10s). After each row, the antenna goes to the following line, starting in the opposite direction. Again, the slew time is encompassed on the first point of each row. One should notice that one row takes longer than the recommended calibration cycle for the Ka-band (even in the more compact configuration). We typically use a calibration every 2 or 4 lines, pushing the interval between the calibration beyond the limit of the acceptable and forcing us to work in exceptional weather conditions. The time spent in a 43x43 calibrating after two rows and pointing after four rows increases the total time of the point-and-shoot observation to 5h47m (20 seconds for each calibration scan and 3 minutes for each

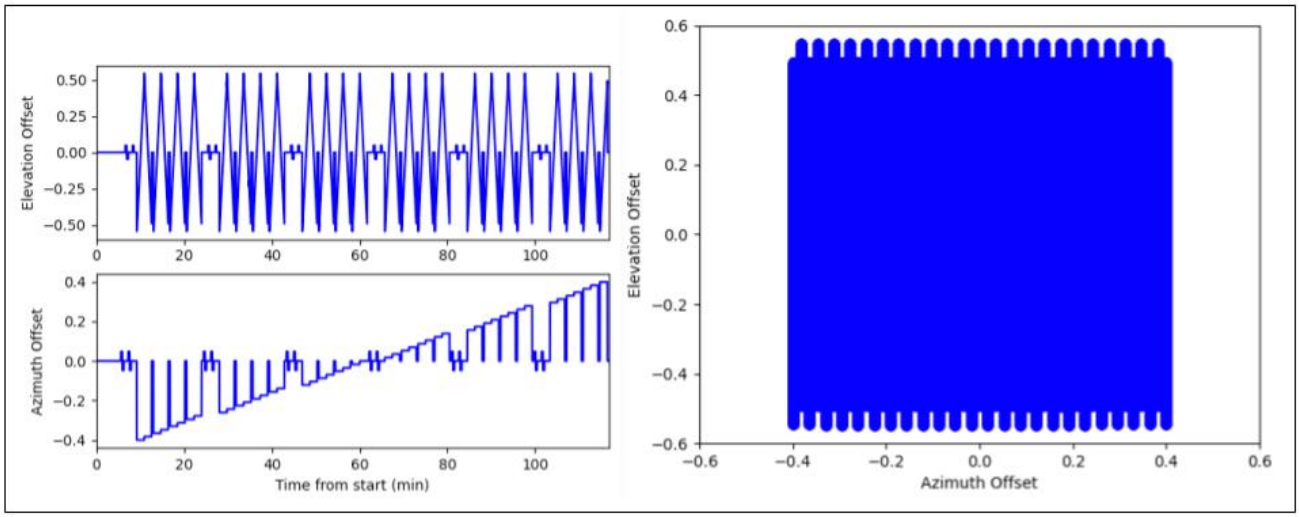

Figure 2: Pointing table of a moving antenna in an OTF holography run. On the left: Elevation and Azimuth changes in degrees on time; notice the calibration of each two rows and the interferometric pointing scan after four rows. On the right: Elevation versus Azimuth plot, where an extra Azimuth offset allows the rump up antenna movement to start the gridding position at the right velocity.

pointing scan). The default oversample value per beam is 1.2 in both directions, meaning the space between the points in a row (and between the rows) is 0.83 beams[1]. Each point in the grid corresponds to a value of l and m that is easy to recover when the antenna stops to perform the measurement.

On the OTF holography, the antenna does not stop to get a measurement, and users need to define the velocity per beam desired. That depends on the target since a bright source only requires a short time on-source to reach an acceptable signal-to-noise. We have tested different speeds before achieving an ideal number. For high frequency (K, Ka, and Q), we suggested 2 seconds per beam, but 1 seconds per beam is an acceptable value for good weather conditions and strong sources ($> 10Jy$). A time shorter than this would require a brighter source that is not quite common in those bands. For the Ku band and below, we suggest 1 second, but we could get high-quality maps using 0.5 seconds per beam for the X-band. In all the cases, we recommend at least 4 points (integrations) in the beam, meaning that the dump time should follow the selected speed: 500ms dump time for 2s/beam velocity, 250ms dump time for 1s/beam velocity, and 125ms dump time for 0.5s/beam velocity.

Since we are doing square grids, the length of each row is defined by the total number of rows and the space between them. Following our comparison between OTF and point-and-shoot, a 43 grid in a 2s/beam velocity for Ka-band would take 76s with a total of 152 interrupt measurements. After each row, there is a dummy subscan for the antennas to go to the start point of the next row, following the opposite direction of the previous one and saving slew time. Once the new row is formed, the antenna acceleration produces some pointing instability, so there is a second dummy subscan before starting to get data.

It is during the second dummy that the antenna rumps up to start the grid in the right place with the requested velocity, as shown in the pointing table graphics of Figure 2. We tested different dummy times before reaching an ideal value of 2 seconds for reaching the start position of the following row and 4 seconds for accelerating and stabilizing the antenna (totaling 82s per row). That reduces the 2-row calibration cycle to 2m44s, the 4-row pointing cycle to 5m28s, and the total time to 1h35m. On the 47x47 grid test for validating the panel adjustments, we used a longer time of 5 and 10 seconds, although it is clear now that those values are too high. Even using these long dummy times, each row on the OTF holography takes 1m31s, which is much lower than the 7m10 point-and-shoot holography. The total map took 1h57m (considering the initial slew time).

The advantage of OTF holography regarding VLA time consumption is quite obvious. There are also other secondary advantages of the high-velocity antenna movement. One particular challenge of the step

[1]On a 47x47 grid with same oversample factor, it takes a total time of 6h24m

Table 1: Time between OTF and Point-and-shoot holography

	STEP	OTF
Calibration Cycle	14m20s	2m44s
Pointing Interval	27m40s	5m28s
Row Duration	7m10s	1m22s
Total Time	5h45m	1h35m

holography is the selection of sources. We do not want the antenna to change the elevation dramatically during the holography because that adds some deformations to the map due to gravitational distortions on the dish surface. We typically observe between 40 and 60 degrees elevation and look for the panel adjustment that optimizes at this elevation. Not many bright sources keep those ranges for more than 6 hours. However, the list of possible targets for holography increases considerably for 1h30s observation, and even 3C84 could be used. There are also advantages related to the weather since decreasing the total holography time avoids changes in wind and temperature, which are more likely to change in a 6-hour interval than in 2. Moreover, shortening the calibration cycle allows better calibration and some flexibility in the weather conditions; although noisy, we could obtain a reasonable Ka-map even during the daytime.

Finally, it is worth making a few considerations about the role of the oversampling parameter on the OTF holography. In point-and-shoot holography, the oversample term defines the space between the points in a row and between the rows. There are two oversampling inputs, one for each direction, and you can deviate from the square grid, explicitly defining different numbers of points to be measured in each direction or setting different oversampling values. On the OTF holography, the oversampling term defines the space between each row (or each column if you think in the elevation movement) since the measurements in a grid line are taken at the dump time scale. In other words, it only means the direction perpendicular to the movement. The size of each row is a free parameter of the OTF routine, and we kept it as an Nrow/oversampling term to make it square.

3 Methodology

3.1 Observations

We have used two methods to validate the OTF holography: (i) we have compared the maps obtained using OTF with those obtained using point-and-shoot holography, and (ii) we made a blind test, asking the antenna mechanics team to displace three panels and check if we could recover the same amount. That last test was similar to the orientation test Rick has described in his memo, but now we would like not only to find the displaced panels but the amount each screw was changed.

We performed our on-the-fly holography observations in the winter/spring of 2024. We did not take new step holography data because, in December 2022, we got a surface dish map from all but one of the 28 antennas. The 2022 data were taken in excellent weather conditions, and we do not expect the panels to show significant changes after one year and a half. After the data was taken in 2022, we had two extra step holography observations done in March and October 2023; the last one was to check a panel adjustment on ea06. Since ea06 data were taken more recently, we initially focused the validation on this antenna using October's 2023 data, but later, we extrapolated the analysis to other antennas using the December 2022 data as a reference.

We first performed many tests to verify if the code Ryan wrote was working properly and to check if it was compatible with our system. Some changes were needed on MCAF and on the executor, which Rich Moeser, Ryan, and Ken have worked on, and we have tested during regular test time[2]. I also made a few beamcut analyses as a verification step. When the procedure was in good shape and we were happy with the results, we performed the tests on February 22nd and March 11th. We kept the same elevation used on step holography, the same band (Ka), and, of course, during nighttime and low wind (less than 5 m/s).

On the first night, we performed two 47-row observations at the Ka-band: one at the expected speed of an on-the-fly holography described in the previous section (2 seconds per beam), totaling 1h57m (including the initial slew time) and another at slow velocity (6 seconds per beam) to focus on reproducing the on-source time of the pointing-and-shoot holography, totaling 3h49min. After the first night, the antenna crew displaced three panels for the blind test, and we performed a new observation in March only with a fast speed (2 seconds per beam).

[2]Vivek Dahwan have actively helped and participated during the initial test phase

On test (i), as I already mentioned, I initially worked on antenna ea06 because it was the one with a more recent panel adjustment, and the data were rechecked in October 2023, but as I will show in section 4, the results were later applied to all antennas that we had scanned. On the other hand, test(ii) was focused on antenna ea16 because during verification, we found a bad panel, totally out of position. The idea was to take a chance that the antenna crew was going to fix the panel and perform the blind test on the same antenna.

The data presented here can be retrieved from the NRAO archive. The name always starts with "otf_holo" and the project is identified under the operations label. It should be easy for anyone who wants to look at the data to locate it using the band and the observation day.

3.2 Data Analysis

I have used AIPS to get the illumination maps and the surface deviation in both point-and-shoot and OTF holography. Simultaneously with VLA OTF validation, I was also working on verifying and validating the AstroHACK software package, a new tool to analyze both steps as OTF holography data in VLA, ngVLA, and ALMA. I was validating only on the VLA part and on the ngVLA needs. Part of the tests used to validate OTF were also used to validate the new software package. Commissioning two things at the same time is never a good idea, so I will present only the results obtained using AIPS here. Eric Greisen and William Cotton made all the required changes to AIPS to read and interpret the OTF holographic mode[3].

The illumination map is not a big issue, and the maps were clearly compatible with each other, as I will show in the following section. As the amplitude scale can be arbitrary (there is no flux calibration), the overall shape of the map was compatible with what is already known. It is worth highlighting that with the on-the-fly movement, we can make high-resolution observations that we could not perform before and explore a few details previously hidden. But in any case, illumination maps are typically easy to understand.

The panel maps require more attention. The primary goal of the holography data is to optimize the surface quality of the dish by making panel adjustments. The validation strategy is to obtain those maps using OTF and the usual AIPS task panel (after running uvhol and holog tasks). The task provides an image and a text file with the amount each screw needs to be moved in inches/1000 (mils, $\simeq 25.4\,\mu$m). The natural question is: how much of a difference in the result for a given screw in two different holo maps (in that case, between OTF and point-and-shoot holography) is acceptable?

As mentioned before and extensively explained in Rick's memo, the VLA antennas are stable in a year timescale. I have used three antennas that were observed in both days of December data to quantify the typical deviation between the screws[4]. It was a simple way to estimate the systematic error of our screw's torque determination [5]. I've obtained an rms of the deviation around 5 mils (127 μm), and I assume 3 times this reference value as a typical error on the torque ($\pm$ 15 mils $\simeq 381\,\mu$m). That means any difference below 30 mils ($\simeq 762\,\mu$m) would be inside the error and would not be a concern for validation.

Summarizing the strategy: I acquired Ka-band OTF holography, and after analyzing the data using AIPS and getting an adjustment map for the screws, I compared the results of the adjustment map obtained using the point-and-shoot technique. If the difference for a given screw were smaller than 30 mils ($\simeq 762\,\mu$m), that would mean an agreement between the methods.

4 Results

The maps obtained during the validation data (grid of 47 rows, oversample of 1.2, producing a resolution element of 80cm on the dish map) are shown in Figure 3, together with the map of EA06 using the point-and-shoot method. The fast OTF map (2 seconds per beam) is presented in the middle column, while the slow OTF map (6 seconds per beam) is presented on the right. The illumination aperture map in volts is in arbitrary units since there was no flux calibration during the observation. We prefer sources that typically have flux density higher than 10 Jy, like 3C273 and 3C279, but eventually, we can use flux with a few Jy and increase the bandwidth by adding more subbands. The source used during the point-and-shoot holography was J0217+7349, and eight subbands of 128 MHz were used to get the map. The OTF data were obtained

[3]Three AIPS tasks were updated in the process: bdf2aips, uvhol, and holog. The bdf2aips changes were made to recognize the extra dummy scans of the OTF holography, while uvhol and holog have new input adverbs to allow the OTF mode.

[4]I decided to scan the 3 most central antennas twice to have them as a sanity check between the two days. The strategy was now useful to making the fluctuations analysis. The antennas are ea08, ea11 and ea25.

[5]The idea of looking for the same antenna twice to quantify systematic errors on the screws torque solution was from Victor de Souza from the AstroHACK team while he was trying to code the software using low-resolution data. I used the same strategy on the high-resolution data we got in 2022.

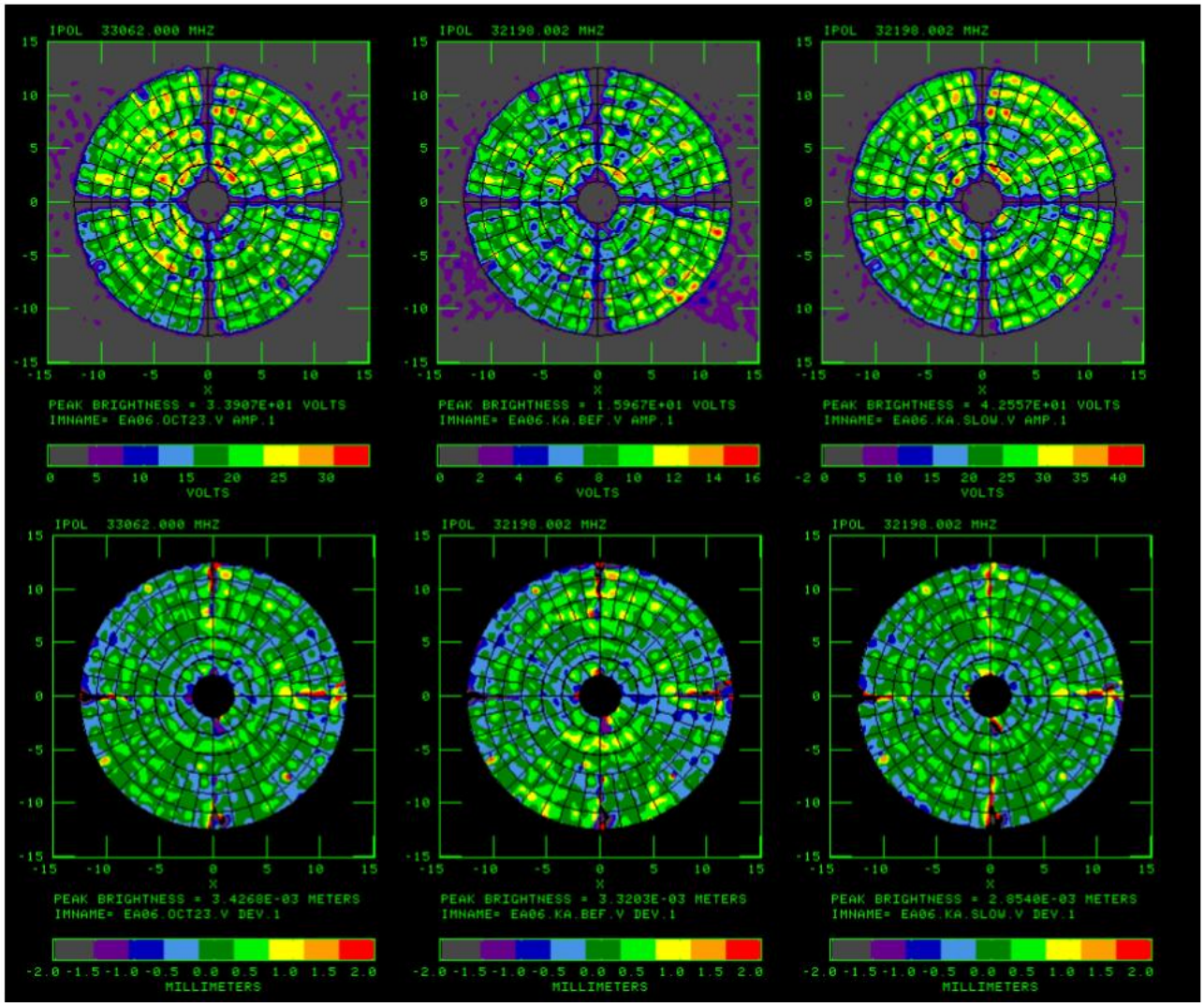

Figure 3: First row: illumination aperture maps of EA06. Second row: Panel deviation map of ea06. From left to right: point-and-shoot results, OTF fast 2s per beam, OTF slow 6s per beam.

using 3C273 during the rise, on a similar elevation of J0217+7349, using only one subband of 128 MHz. That explains the difference in amplitude. Please notice that although the illumination looks more uniform on the point-and-shoot, most of the features present are observed: the upper panels of the innermost ring are positive, the four bright panels on the fourth ring on the top-right quadrant; a loose panel with weak emission on the bottom-right quadrant (fifth ring).

The accuracy of the dish deformation measurement can be computed using equation 25 of Rick's holography memo(EVLA Memo 212). The fast OTF holography has the disadvantage of spending less time on the source, although that is compensated by using brighter sources, as explained in the previous section. On the slow OTF, we set the time on the source to be equivalent to the point-and-shot holography. The signal-to-noise ratio of each of the ea06 observations presented in this report is shown in Table 1. The values reached were close to the theoretical, considering the target's flux density $\sim$ 20 Jy for the OTF (3C273) and $\sim$ 5 Jy to the step (J0217+7349), the used bandwidth, one reference antenna, and the system temperature at Ka band. We also present the surface rms obtained on each run and the accuracy of the measurements. The surface rms between step and February OTF observations agree inside two sigma, which is a convincing argument favorable to validating the OTF method.

Table 2: The SNR, surface rms, and holography accuracy for ea06 on the different measurements.

Observed Day	Year	Type	On-source time	bandwidth MHz	SNR measured	SNR expected	rms-surface μm	accuracy μm
October 7th	2023	STEP	6s	800	40	45	330	20
February 22nd	2024	OTF	2s	100	130	120	380	6
February 22nd	2024	OTF	6s	100	200	210	350	4

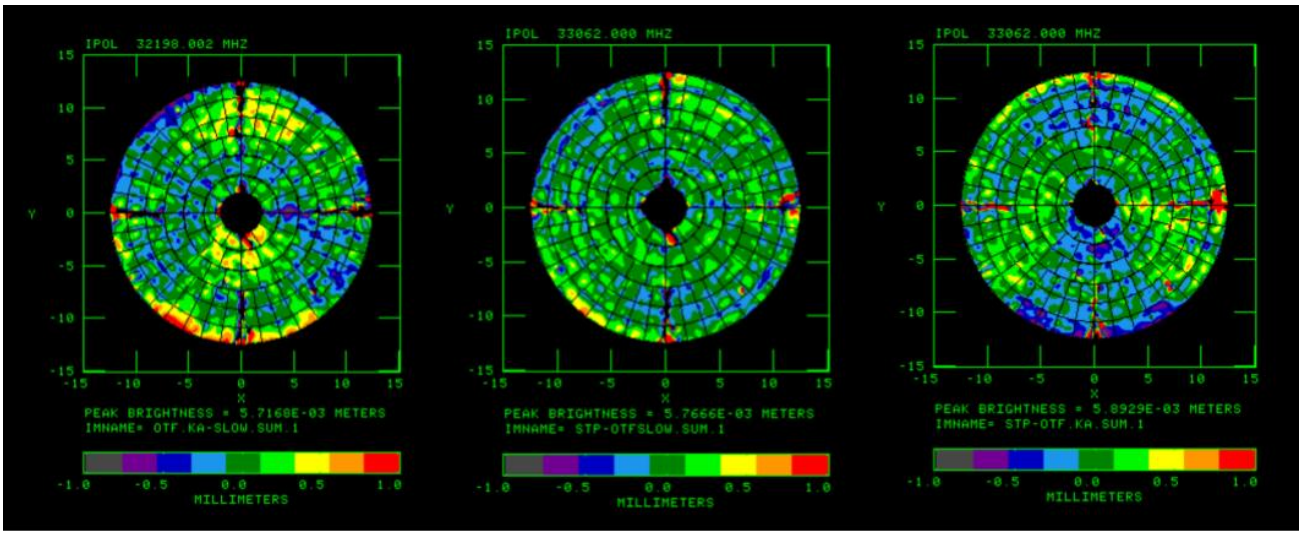

Figure 4: Left: Subtraction of the panel deformation map obtained with step holo and 2s per beam OTF (residuals rms of 463 μm). Middle: The same between step holo and 6s per beam OTF (residuals rms of 422 μm). Right: the same between the two OTFs maps (residuals rms of 520 μm).

The reader should notice that all the features that are presented in the left column of Figure 3, which correspond with the point-and-shoot holography, are presented in the middle and on the right columns, which correspond respectively to the fast and slow OTF holography. However, some features are more evident in the fast OTF data and others in the slow OTF. The reason for this is the difference in elevations between the holos; the VLA panels change significantly depending on the elevation[6]. I tried to use the same elevation, but it is challenging to reproduce all the deformation changes that happen during 6 hours in a short-term run. The idea of running a slow OTF observation was to reproduce the elevation changes during movement, but even considering the same on-source time, the total map took much shorter because there was no need for the antenna to stop. Notice that each OTF map is more coincident with the point-and-shoot map than between them because since one was done after the other on the same day, there is no elevation overlap between them. Each OTF observation was done at a totally different range, while the elevation range of the point-and-shoot mode encompasses the elevation range of both OTF runs.

In Figure 4, I show the differences between the step holo map of the dish deformations and those from OTF (left). In the middle, I show an equivalent figure replacing the 2 hours OTF with the slow 6 hours OTF, while on the right, I compare both OTFs. Noticed that the differences in the dish deviation are less than 1mm (between -0.5 and 0.5 mm).

In Table 3, I present a quantification of the discussion presented above, also to avoid a false impression of disagreement due to the color scale. It shows the agreement rate of 11 antennas (from the 15 antennas scanned, 3 of them were too noisy, and the other one did not have a good step holo to use as a reference). I defined the agreement rate between two deformations maps based on how many torque solutions for the total of screws are equal, where equal means differences inside the estimated error of 15 mils (0.38mm).

I have looked screw per screw of the OTF data and subtracted from the value obtained using the point-and-shot mode. For every absolute difference higher than 30 mils (0.76mm), I identified it as a non-match re-

[6]In a test made in October 2022, I performed point-and-shoot holography on 3C84, and the change in elevation provided a clear signature on the panel maps when compared with the holographic measurement taken at medium-degree elevation.

Table 3: Comparing OTF and Point-and-shoot holography

Antenna	pad P&S	pad OTF	% of agreement	mean deviation mils / mm	Antenna	pad P&S	pad OTF	% of agreement	mean deviation mils / mm
EA03	E10	E06	97.98	6.28 / 0.16	EA06	W01	E10	99.80	7.29 / 0.19
EA08	N01	N14	96.37	8.06 / 0.20	EA09	W06	W02	96.57	8.59 / 0.22
EA13	W16	W14	95.56	8.65 / 0.22	EA15	N16	W16	95.36	7.98 / 0.20
EA16	E06	E02	98.99	6.68 / 0.17	EA18	N14	N18	94.15	9.89 / 0.25
EA22	N02	N06	98.98	6.98 / 0.18	EA25	E02	E14	97.77	9.30 / 0.24
EA26	W12	W10	95.97	9.89 / 0.25	ALL			96.54	8.43 / 0.21

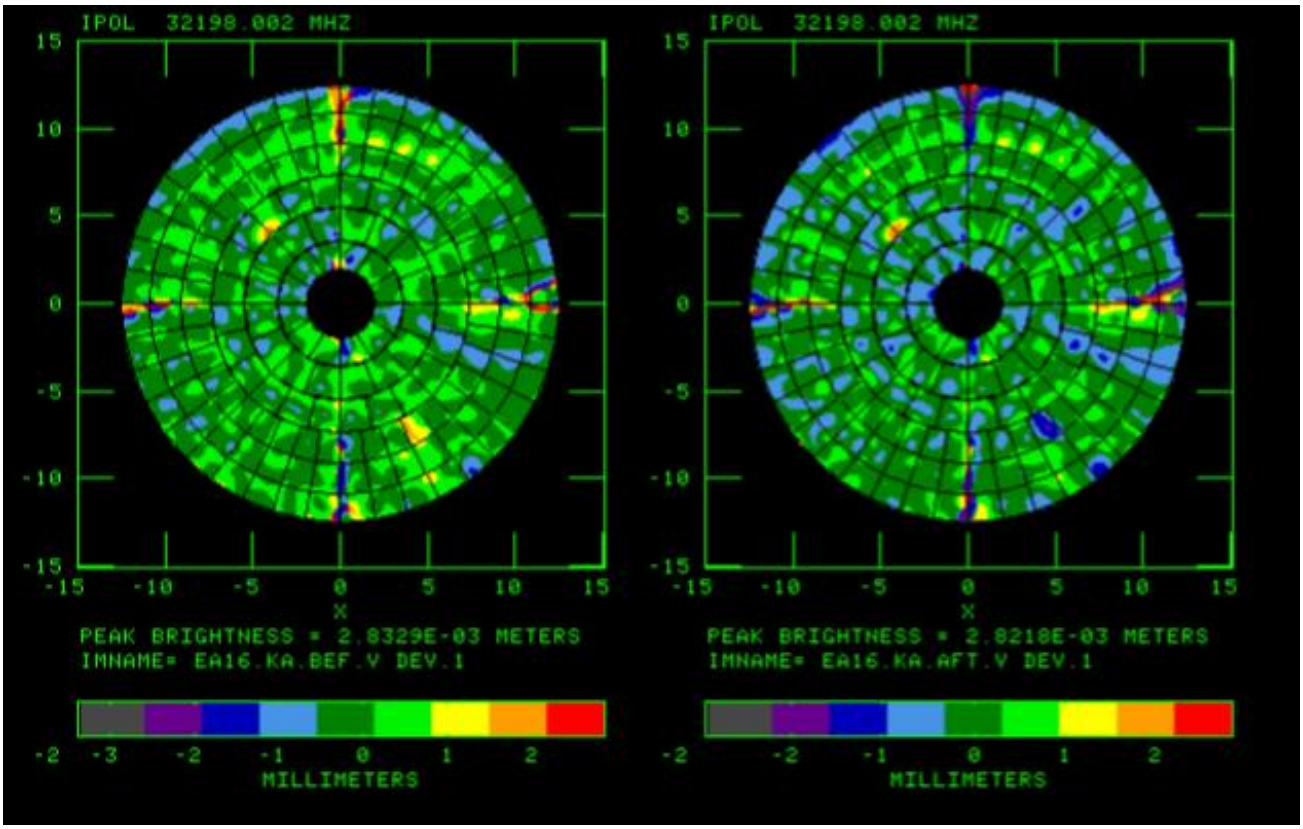

Figure 5: EA16 before on Feb 22 (left) and after on Mar 11 (right), the antenna mechanics team displaced 3 panels. The small amount is not clearly seen by eyes, but the lousy panel of EA16 is evident on the fourth ring (bottom-right quadrant).

sult. I have excluded screws on panels in the shadow of the arms, leaving 492 screws per antenna to check the agreement. The table shows that 97% of the screws are in agreement between the two holographic modes. The scale is so tiny that even at VLA, we could feel minor changes after two years. For antenna ea06, the only one having a map in less than six-month intervals, the agreement was higher than 99%, i.e., only one screw in disagreement between both OTF observation (fast and slow) and the step mode holography[7].

Since the results of the first night of tests were satisfactory, we could proceed to the second step of the validation: the blind test. Kelly Greene and the antenna's mechanics team displaced the panels on March 03, and I made a new Ka-band holography on March 11 to recover the amount his team made in each screw.

[7]At the level of 15 mils, the antennas may slightly differ depending on the subband, although the solution stays around 95%. For all antennas but ea06, I used the spectral window at frequency 33.1 GHz to compare OTF and point-and-shoot. Since ea06 was in a weak source on the point-and-shoot, I needed to use the eight subbands to get a good panel map. I prefer to use the lower frequency on the OTF data (32.1 GHz) to compare with the 800MHz bandwidth combined with the point-and-shoot. Comparing with a different subband will decrease the number to 98.79% (6 screws)

The amount displaced in each screw was below the error estimation I made in section 3. That made the test challenge the limit of our capabilities. Nevertheless, we could find the amount the team added despite having a false positive detection: one panel was close to the limit of the errors. The false positive could be a consequence of the lousy panel close by, but at his point, that is only speculation. On the positive side, we could recover the amount of torque the antenna crew set in each screw even when they did an amount lower than our errors, which could lead to a conclusion that perhaps I have overestimated our errors. Here is the summary of the results:

- panel 3-16 I found the team added 12.0 12.0 -12.0 -19.0. The team put 15 15 -15 -15
- panel 5-36 I found the team added -11.0 -14.0 -6.0 -19.0. The team put -20 -20 -20 -20
- 4-6 I found the team added 23.0 15.0 18.0 8.0. The team put +20 +20 +20 +20

A positive sign means lowering the panel away from the sub-reflector, while a negative sign means raising the panel toward the sub-reflector. The screw order presented is: inner-edge-left/inner-edge-right/outer-edge-left-outer-edge-right. The maps before and after are shown in Figure 5.

5 Applications

As pointed out in the previous sections, the OTF holography has several advantages, such as shortening calibration cycles and decreasing the total observation time. That allows us to apply it to get holography measurements on more flexible conditions than point-and-shoot holography. In this section, I will show wide-extension holography done at the X and Ku bands, daytime holography at the Ka-band, K-band holography at the A configuration, and the best attempt to get a Q-band surface map.

We obtained two high-resolution maps at X and one at Ku bands shown in Figure 6: a VLA dish in a way never seen before. We were able to increase the antenna scanning speed for the X-band measurements and obtain a map with 119 rows and a resolution of 32 cm on the dish. Notice that the contribution of the sub-reflector produces changes in the surface deformation maps between X and Ku. That happens because the map is computed based on the phase measured at each point (resolution element). Since the radiation reaches the sub-reflector first, it introduces an error on the phase presented as large signatures on the surface maps. At the VLA, the sub-reflector rotates depending on the band, which is the large deformation seen in the maps that also rotates depending on the band. In principle, that could be considered and removed from the map, but there was not enough information to describe it before the OTF holo allows high-resolution maps on low-frequency. An additional discussion needs to be conducted on the overall surface rms determination.

The surface rms measured at X-band at the VLA antenna is two times higher than at Ka-band in both pointing-and-shoot and OTF holography. That fact has never been explored before, and it is unclear if that is real since X-band efficiency is higher than Ka-band efficiency. In Figure 7, I show the 119 rows OTF maps side-by-side with the X-band 43x43 point-and-shoot data obtained in 2014[8]. There are no significant differences other than the resolution on the aperture plane. In general, both maps show deformations inside 2 mm and the same lousy panel, indicating it has been there since 2014.

The surface rms on the pointing-and-shoot holography of 2014 is 680 μm, while the most recent X-band OTF data shows a surface rms of 770 μm. The EA06 data at the Ku-band, shown in Figure 6, also presents a surface rms of 675 μm, and it is more compatible with the X band than with the Ka-band. When we look at the phase maps apertures[9], the phase rms are twice as high at Ka-band than at X, while the wavelength of the subbands analyzed is almost 4 times minor at Ka (0.9 cm) than at X (3.2 cm). That would explain why we are getting surface rms twice as high at the X-band, but it does not explain why we are getting phase rms on the image aperture so high . Further investigation out of the scope of this memo will be required.

In Figure 8, I show the results of the first tests at the Ka and Q bands, highlighting that we could get a reasonable map at the Ka-band even during daytime. I have tried several times to get a reasonable map at Q-band, which was always challenging using point-and-shoot holography. I had the best results during a night observation and good weather conditions (low wind, no clouds).

In his Memo (EVLA Memo 212), Rick showed in Fig 15 and 16 the surface deformations X to Q band using point-and-shoot holography, discussing the band-to-band differences between the maps. That is similar

[8]Rick Perley provided to me the calibrated data

[9]I have exported the amplitude, phase, and deviation maps to a fits file and asked Victor de Souza from astroHack to check those values outside any software package. We did not consider the rms on the leg's shadows

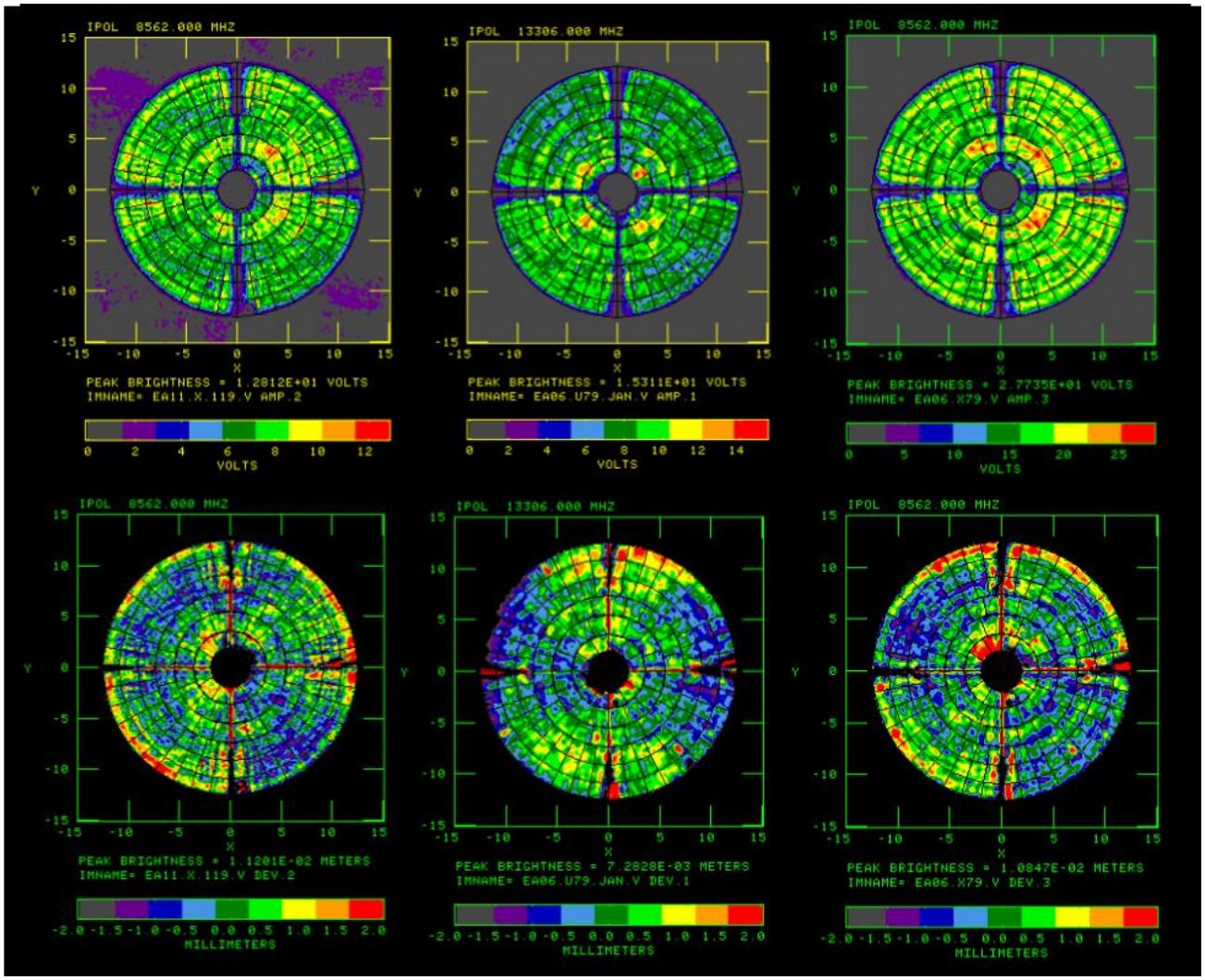

Figure 6: Since the OTF technique allowed us to get a panel map much faster, I could try large holos at the X-band and Ku-band to see high-resolution maps of the VLA dishes with enough signal-to-noise to resolve each detail. Top: Illumination aperture map, bottom: panel displacement map. Right to left: EA11 X band 119 rows on Feb 12 (resolution element of 32cm), EA06 Ku band 79 rows on Jan 12 (resolution element of 48cm), and EA06 X band 79 rows on Jan 7 (resolution element of 48cm). All data from 2024. Since I scaled the extension of the raster using the beam size, the same number of rows produces the same resolution on the surface map for X and Ku bands (see Mangum et al. 2022, ngVLA memo 12, euqation 1). I got all the data during the daytime on test days.

to what we have here on the OTF holography. In particular, we can compare the noise maps of the Q-band data to highlight the challenge of getting the surface deviation map on this high-frequency band.

Finally, I could also use OTF for a holographic measurement during the extended configuration. It is indeed not easy and not appropriate, but during the BnA to A configuration move last fall (October 7th), I tried an OTF holo at K-band during daytime. I tried a low-resolution observation (to fit the gaps better) of 27 rows in 2s per beam speed, but at the end I have run it during a good weather test time (around 10 am), using a calibration cycle of 1m57s and a pointing cycle of 7m40s. I will focus the results on the illumination aperture since the resolution was too low and phase condition was not ideal to discuss panels displacements.

In Figure 9, I show the illumination pattern at the K band for the antennas of the North Arm, already in the A configuration position. Antenna ea17 was at N16, and I used baseline with ea23 at N08. Antenna 10

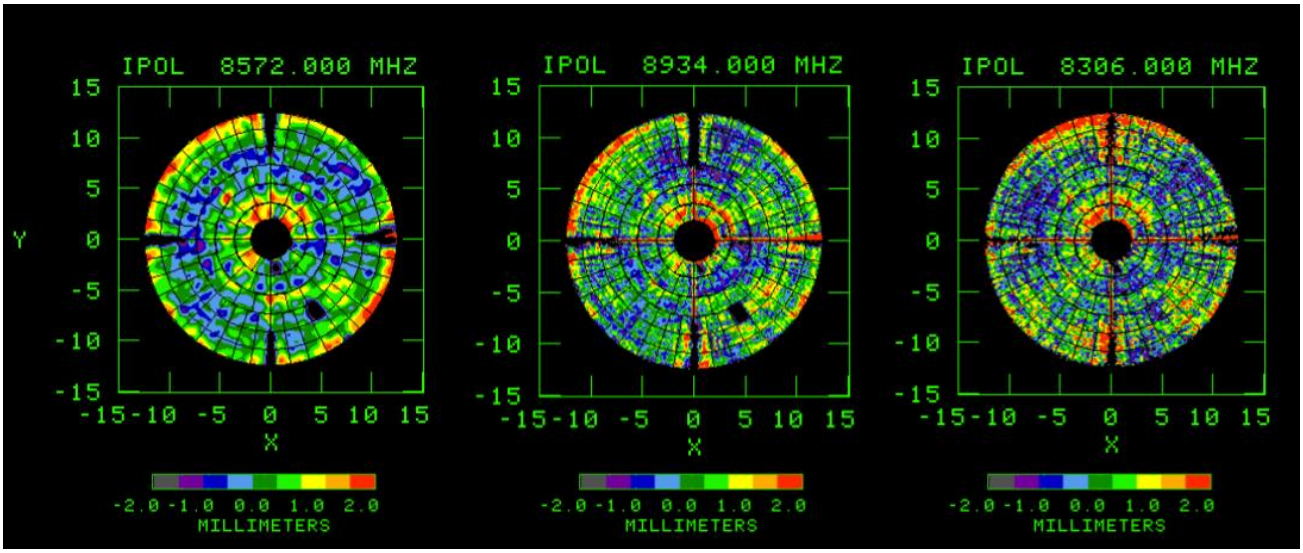

Figure 7: EA16 surface deviation on three maps. Left: 43x43 Point-and-shoot holography done in 2014 (Dec 31). Note that the louse panel is already on the fourth ring. Medium: 119 rows otf holo done in 2024 Feb 8. It clearly reproduces the same pattern as 10 years before. Right: 119 rows OTF holo done on Mar 18, after the blind test. The surface slightly changed on the top edge. The louse panel was still there, but it floats with elevation. The panel was fixed on June 12. Most of the other structures remain the same except for the fixed panel.

was at N48, and I used baseline with antenna ea07 at N56, and for antenna ea22 at N64, I used ea18 at N72, the farthest antenna in the arm, as a reference. The calibration cycle was each two lines. After that run, I tried 47 rows during night, but unfortunately, it could not fit in any gap before the start of A configuration.

Although those are not the best maps already made for a VLA antenna, the results look promising in an attempt to get holography maps on extended configuration. Of course, D and C configurations are always the proper choices for high-resolution and high-sensitivity holography maps. Here, I am only stating that the OTF technique allows us to take those measurements in various situations that were not possible before.

A final helpful application for the support telescope that was not discussed is the possibility of using the OTF holographic mode to perform fast beamcuts to diagnose issues in focus, pointing, and other related optics problems that downgrade performance. Beamcuts were already done a few times with the usual pointing-and-shoot holography mode, like on the interesting subreflector alignment analisys on Memo 211 (Perley et al. 2021). However, now, we can do it faster, depending on the source brightness, to allow enough signal-to-noise, as we did in the EVLA Memo 228 at 4-band (Vydula et al. 2023). We are already using it to check the optics status, although a final change in the procedure would be needed to remove the pointing scan properly, depending on the situation.

6 OTF Holo Script

The OTF holography mode is not yet available on OPT, and at the moment I am writing this memo, it can only be used outside the OST and the dynamic schedule. It has some similarities with the input parameters used in the point-and-shoot holography. The user can choose the time spent on the calibration and in the pointing scan and can define the calibration cycle. It is possible to define the inclination of the first scan, which is a valuable tool for low-frequency beamcuts (see again EVLA Memo 228).

The most important parameters are the speed, in units of seconds per beam, the number of rows, the oversampling between the lines, and the size of each line in beam units (FWHM). As already explained in section 3, we used the number of rows to constrain the line length in a way that produced a square grid, but that can be changed (as we do for beamcuts).

Below, I show one example of the inputs needed for the square grid. Those input variables are at the beginning of the script to make it easier for everyone who wants to try. The only caveat is that the integration time needs to be the same as the dump time used on

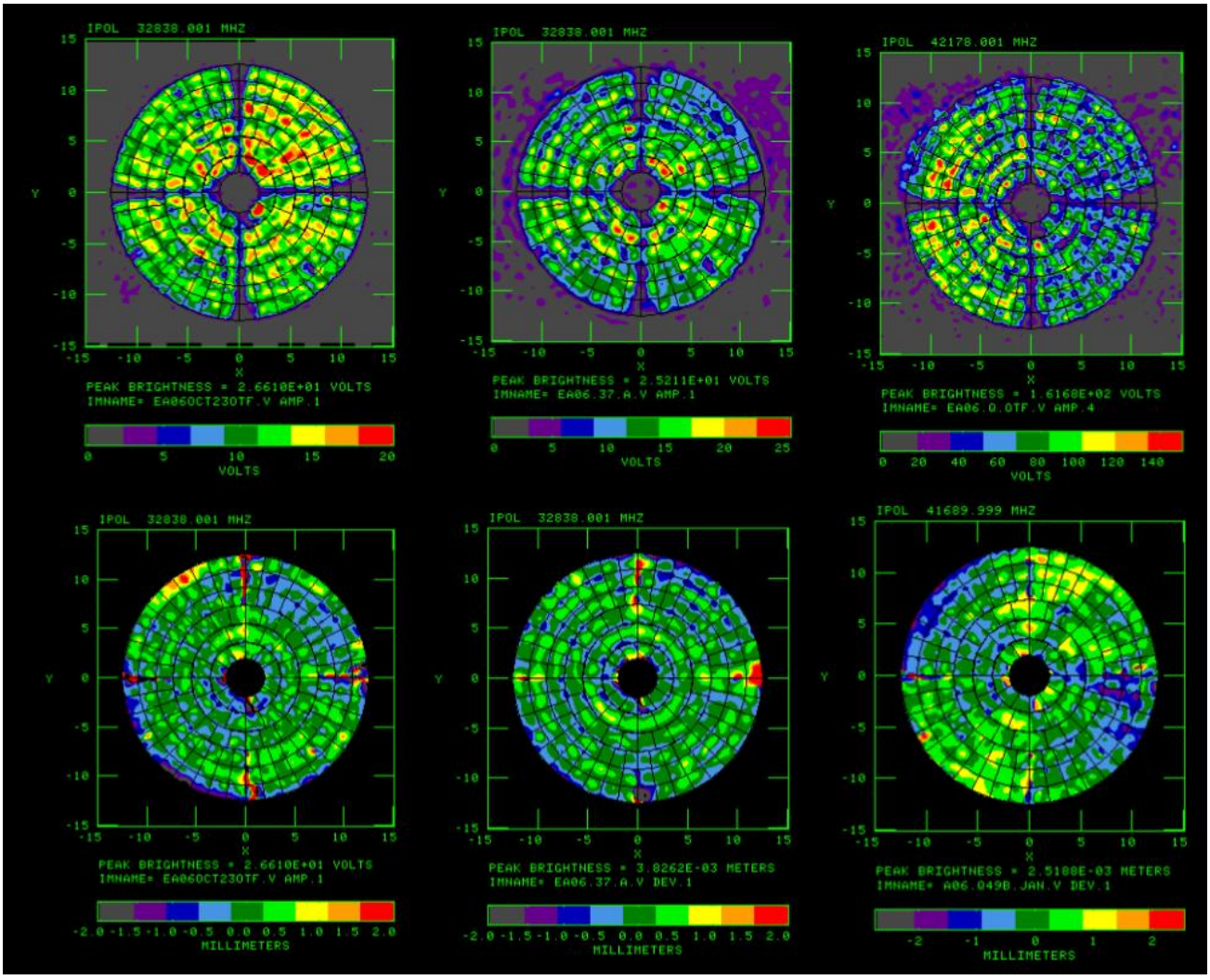

Figure 8: The first OTF holography maps at Ka and Q bands for EA06. Top: illumination maps. Bottom: Panel displacement maps in mm. Left to right: Ka-band 47 rows map during the night time (data taken on Oct 21, 2023); Ka-band 37 rows during day time (Oct 12, 2023) and Q band 47 rows during night time (Jan 16, 2024). We show here that even daytime holography at Ka-band is now at least possible, although not recommended: the image is still too noisy. And even with OTF, the technique is still challenging to get a Q-band holo map. I show the best attempt here in perfect night weather.

the RCT. That will also impact the input integrations per sub-scan. In the square grid situation, we only need to define the cycle of calibration and pointing (in units of rows), the number of rows, the time in seconds on the beam, the time on the calibrator and the pointing scan, the oversample, and the dump time.

Ncal = 2 # calibration after the Nth row

Npnt = 8 # pointing after the Nth row

Nrow = 47 # Number of rows (square grid)

ts = 2 # time in second per beam

tcal = 20 # time on source for calibration in seconds

tpnt = 180 # time for pointing scan in seconds

over = 1.2 # oversample the beam between the lines

tdump = 0.5 # dump time in seconds

refnums = [1,4,27] # antennas used as reference

Certainly, one does not need to follow the square grid. Below, I will show an example of how we call the OTF holography, and one can adapt and add it to

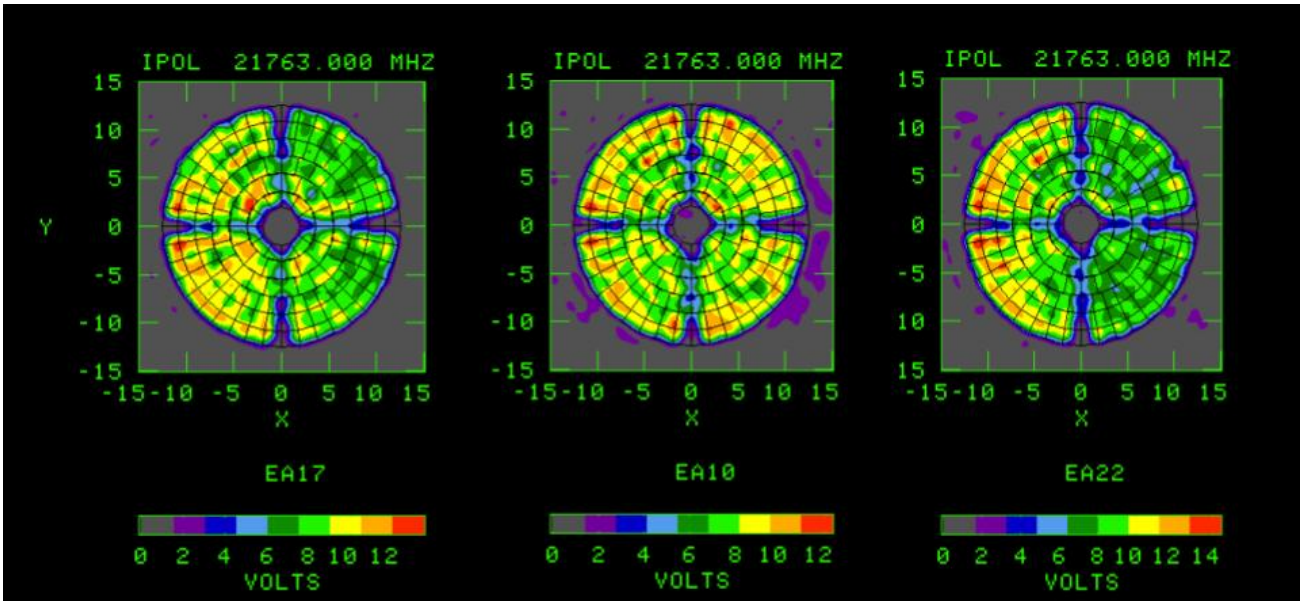

Figure 9: A low resolution 27 rows OTF holography map at K band for antennas on the north arm in A configuration position (left to right: EA17, EA10 and EA22). Pointing scan were made each 7m40s and the calibration cycle was 1m57s.

a different script[10] as needed. As in a regular observation, you first need to define a correlator setup for your scans. The pointing data does not need to have a short dump scale like the vci file used for the holo. For example, let's use the setup I used for the Ka-band observations:

loif_x = LoIfSetup(True, F_p, 8460, 0.0, 8588, 0.0, 0)

loif_x.setWidarOffsetFreq(0.0256, 0.0256, 0.0, 0.0)

loif_a = LoIfSetup(True,F_h,33520,0.0,32520,0.0,0)

loif_a.setWidarOffsetFreq(0.0256,0.0256,0.0,0.0)

vci_a="/home/mchost/evla/scripts/test/otf_holo/
THIG_short_tdump_ka.vci"

vci_x_pnt="/home/mchost/evla/scripts/test/
otf_holo/band_x.vci"

band_a = OtfHoloBand("A", loif_a, vci_a)

band_x_pnt = OtfHoloBand("X", loif_x, vci_x_pnt)

where F_p and F_h are the pointing and holography frequency respectively, and in our case was "10GHz" and "33GHz". Then, you need to define the calibration scans, as:

cal_spec = OtfHoloCalSpec(src, band_a,
interval=Ncal, duration=tcal/86400.0)

Where src is the source coordinates, band_a is the band object defined using the vci file, the interval is the number of rows between two calibrations scans and duration is the duration of the scan in days. Then, you will need a similar command for pointing:

refp_spec = OtfHoloRefpSpec(src, band_x_pnt,
interval=Npnt, duration=tpnt/86400.0,
fn=vlaPointing)

Where band_x is the band object defined using the vci file, the interval is the number of rows between two pointing scans and duration is the duration of the pointing scan (minimum of 2m30s). The fn calls the usual VLA routine for pointing - we did not test something different than that. The other inputs remain with the same meaning. Then, you need to set up the holoraster scans.

holo_spec = OtfHoloScanSpec(src, band_a,
int_time=tdump/86400.0, ints_per_subscan=4,
dummies=2)

[10]You will need to add execfile('/home/mchost/evla/include/otf_holo.py') and execfile('/home/mchost/evla/include/onsource.py') on top of your code

Where again src has the same meaning as above, band_a is the correlator setup for the holoraster (short dump time), integration time that needs to be the same as the vci file dump time in days. The ints_per_subscan defines the length of each subscan, set as multiples of tdump. In our tests, we reached an ideal number of 2 seconds, meaning 4 integrations for this particular example. Finally, dummies define the number of subscans before each row. There is also one dummy subscan after each row, so two means a total of 3. Given a subscan duration of 2 seconds, this leads to 6s of extra time per row as mentioned in Fig. 2. We do not recommend using time shorter than that for usual high frequency holography. Using longer would produce a waste of time, but it will not corrupt your data. However, for long wavelengths beamcuts like the P-band, you must increase the time to allow the antenna to arrive at the start point after each calibration cycle. You can now generate your scans as:

scans = holospec.make_scans(beam_time=ts/86400.0, beams_per_scan=Nrow/over, beams_bw_scans=1/over, num_scans=Nrow,rot_deg=0)

Where beam_time is the time in days taken to move one beam width (FWHM). Remember that the antenna does not stop, and as shown in figure 1, the ideal number is to have at least 4 integrations per beam (ts equal or higher than 4 times the dump time). Beams_per_scan define the scan length in beam units. Here, I show the example of a square grid, but the user can select any value if the square is not desired. The beams_bw_scans is equivalent to the oversample on the usual holography, and it tells the separation between the rows in beam units. The num_scans define the number of rows while the rotdeg defines the direction of the movement, where 0 means elevation (starting bottom to top).

Then, you need to create an OtfHoloExecutor object, which will handle the row, calibration, and pointing scans:

exe = OtfHoloExecutor(array, subarray, myPrint, printTime, waitOnSource)

This call includes a setup scan so the antennas will arrive on source before starting the grid (it will start after half of the reference antennas arrive on the source). Finally running as:

mjd = exe.otf_holo(scans, refstrs, holo_spec, cal_spec, refp_spec, array.time(), 12.0/24)

where the scans, holo_spec, cal_spec, refp_spec are defined above and array.time is the time to start executing (now). The refstrs is a list of antenna id strings (e.g. "ea09") to use as references, generated from refnums. The last input, showing here as 12.0/24 is the maximum time in days allowed for the holo run. In this case, if the grid takes longer than 12 hours, it will be interrupted. That is reminiscent of the point-and-shoot holography when an ad hoc time cut-off was added to avoid very large grids in case of miscalculation of the total time. It is not a quite useful input for OTF, and leaving it as 12 will allow most of the situations. Once complete, the call returns a time for the end of the final calibration scan, which can be used as an execution start time for any additional scans.

7 Conclusion

I have presented the validation test of the OTF holography for the VLA, a faster method to obtain a surface dish map and get panel optimization. The method reproduces satisfactorily the results obtained with the usual point-and-shoot holography. It opens a new window for the VLA since we will now be able to obtain high-resolution maps in all bands and verify structures that have not been resolved before. It will also be necessary for the ngVLA prototype antenna and will be able to characterize eventual dependencies of the dish deformations with the elevation.

The OTF data can be reduced using AIPS thanks to the updates made on the 2023 AIPS version, and it will also be possible to use the astroHack Python package soon. All the tests presented here were also analyzed using astroHACK, and things are moving fast. A future memo validating astroHACK will be written.

Acknowledgements

I have written the present memo and worked on the validation during the past year, but that is not a one-man job. The result presented here, along with the progress made on the development of the new tool to get fast maps, is a result of a team effort and is only possible due to the high dedication of my colleagues. I would like to acknowledge the work done by Ryan Berthold on implementing the on-the-fly holography and caring about each detail, and also Ken Sowinski, Rich Moeser, Eric Greisen, and Bill Cotton for making the changes on diverse software to make data acquisition and analysis possible. Ryan also revised the manuscript text, which I really appreciate. I also thank the help of Vivek Dhawan and Paul Demorest during the testing time and all the fruitful discussions I had with Jeff Mangum in the past months. Jeff provided valuable comments on the writing that increased the overall scientific content

of the memo, acting either as an assiduously reviewer and as a kind referee. I thank Rick Perley and Bryan Butler for their suggestions and insights during testing and all the astroHACK team (Jan-Willem Steeb; Victor de Souza; Joshua Hoskins, Josh Marvil, and Urvashi Rao Venkata) for the close collaboration on developing a new tool to analyze the data simultaneously to the validation process of a new technique. I particularly thank Victor for a closer look at the X-band surface rms.

References

[1] Baars J. W. M., 2007, ASSL, 348. doi:10.1007/978-0-387-69734-5

[2] Baars J. W. M., Lucas R., Mangum J. G., Lopez-Perez J. A., 2007, IAPM, 49, 24. doi:10.1109/MAP.2007.4395293

[3] Bennett J. C., Anderson A. P., McInnes P. A., Whitaker A. J. T., 1976, ITAP, 24, 295. doi:10.1109/TAP.1976.1141354

[4] Buffa F., Serra G., Poppi S., Egron E., Murgia M., Pinna A., 2020, SPIE, 11445, 114456G. doi:10.1117/12.2561787

[5] Cassanelli T., Bach U., Winkel B., Kraus A., 2024, A&A, 687, A27. doi:10.1051/0004-6361/202142116

[6] Kesteven M., 1994, JEEEA, 14, 85

[7] Mangum, J. G. 2022. ngVLA Antenna Memo 12

[8] Mangum J. G., Baars J. W. M., Greve A., Lucas R., Snel R. C., Wallace P., Holdaway M., 2006, PASP, 118, 1257. doi:10.1086/508298

[9] Morris D., Baars J. W. M., Hein H., Steppe H., Thum C., 1988, A&A, 203, 399

[10] Nikolic B., Prestage R. M., Balser D. S., Chandler C. J., Hills R. E., 2007, A&A, 465, 685. doi:10.1051/0004-6361:20065765

[11] Perley, R. 2021, EVLA Memo 212

[12] Perley, R., Sowinski, K., Wilkins, L., Andersen, S., 2021, EVLA Memo 211

[13] Serra G., Bolli P., Busonera G., Pisanu T., Poppi S., Gaudiomonte F., Zacchiroli G., et al., 2012, SPIE, 8444, 84445W. doi:10.1117/12.926160

[14] Tarchi D., Comoretto G., 1993, A&A, 275, 679

[15] Vydula, A. K, Bowman, J., Jacobs, D., Schinzel, F., Tremou, E., Beaklini, P.P.B. 2023 EVLA Memo 228